Controllability Analysis of an Ethanol Water Distillation Coloumn

Willem Adriaan Smit
14052131

CBT

2019-05-13

Controllability Analysis of an Ethanol Water Distillation Coloumn

Willem Adriaan Smit

14052131

Department of Chemical Engineering
University of Pretoria

CBT

2019-05-13

Controllability Analysis of an Ethanol Water Distillation Coloumn

Synopsis

Welcome to the Noob's guide. This section has only been included for reference on how to use it when comparing the source code to the resulting document. Please continue to the Introduction, Section **??**.

Contents

List of Figures

List of Tables

1 Introduction

Renewable energy is becoming a major role player in the world today. As people are starting to shift away from fossil fuel based technology and energy generation, the focus is shifting to alternative methods of energy (and fuel) production.

One such a method involves the use of ethanol as an alternative fuel. Ethanol particularly is an excellent contender for a major alternative fuel, as it can be produced from crops or by means of biological fermentation. [A lot of] research is currently done on methods to generate ethanol in order for it to power the future.

Producing ethanol, however, is not the only problem to overcome. After the production process (usually from fermentation), the ethanol has to be separated from the product mixture in order to purify it. This poses to be a challenge (and a very energy intensive operation) due to the thermodynamic properties of the homogeneous mixture between water and ethanol. As noted in Figure 1, the system contains an azeotrope. This leads to very expensive separation operations, as pressure swing distillation has to be implemented for high purity separation.

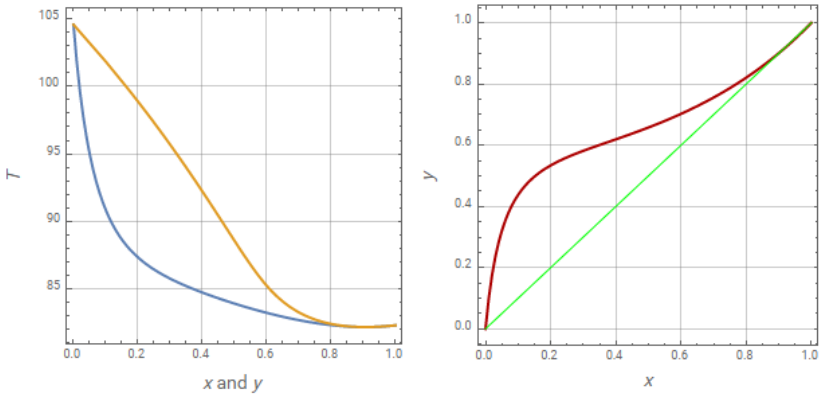

Figure 1: Vapour Liquid Equilibrium (VLE) data for the water ethanol system at 1 bar.

In this report, an investigation regarding the controllability of the ethanol water separation process is investigated. The plant investigated is a pilot plant that is testing the feasibility for scale up of the process. Control has to implemented to ensure that the system reaches a steady state, as well as to improve the overall profitability by reducing the standard deviation in the product quality.

A plant wide control system will not be investigated. Only the distillation coloumn is analysed. The current proposed control system is discussed in Section [REF!!!]. This report will investigate the validity of such a proposed control scheme, as well as the where the physical constrains in the system lies.

2 Process Model Description

2.1 System Diagram

The Process Flow Diagram of the system, with all the relevant inputs, outputs and disturbances are displayed in Figure 2.

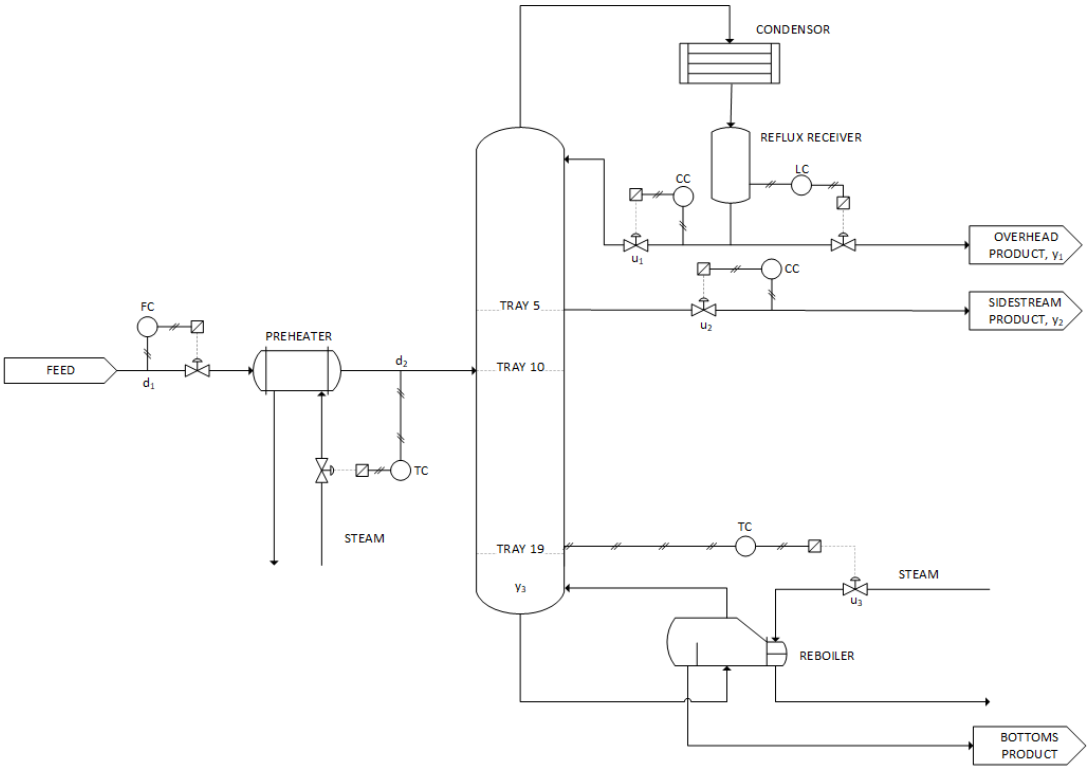

Figure 2: Process flow diagram of the system

2.2 System Description

The system involves the separation of water and ethanol (in a solution), with the aim of producing an ethanol product that can be used as an alternative fuel source.

The system can be summarized as follows:

- The distillation column of the pilot scale plant is a 19 tray, 12 inch diameter column.
- The column has variable feed and side stream draw off locations.
- The side stream flow is varied to control the composition of the stream.

- The distillate vapour draw off stream is fully condensed, and then separated into the reflux and product streams.
- The product stream is set to control the level in the condenser, while the reflux stream controls the composition of the distillate product.
- A kettle re-boiler is used to add energy to the column. Stream is the main utility.
- The amount re-boiled bottoms product is controlled by varying the steam supplied to the re-boiler.
- The feed temperature and flow rate can be controlled to simulate disturbances on the system. These variables are strictly defined as disturbances, as they are part of another section's (the bio-reactor or chemostat) control scheme.
- Currently all variables are controlled with single input single output (SISO) control loops.

2.3 Measurement of Variables

The compositions are measured/determined through various on-line sensors (densitrometry and refractometry). Temperatures are monitored using thermocouples. Flow rates are measured with thermal mass flow meters. Levels are measured by inference from static head, measured with a pressure sensor. The product model and serial numbers are not available.

2.4 System Variables

All variables in the ethanol water distillation coloumn system is summarised in Table 1. The current steady state values hold reference to the tested conditions on site.

Table 1: Summary of all the model variables.

Input Variables			
Variable	Description	Steady State Value	Units
u_1	Reflux flow rate	0.18	gpm
u_2	Side stream product flow rate	0.046	gpm
u_3	Reboiler steam pressure	20	psi
Output Variables			
Variable	Description	Steady State Value	Units
y_1	Overhead ethanol mole fraction	0.7	-
y_2	Side stream ethanol mole fraction	0.52	-
y_3	Tray #19 temperature	92	°C
Disturbance Variables			
Variable	Description	Steady State Value	Units
d_1	Feed flow rate	0.8	gpm
d_2	Feed temperature	78	°C

2.5 System Model

The model was determined by conducting pulse testing on the system. In most cases a first order plus dead time model gave a sufficiently accurate fit to experimental data. The sum of squares of an adequate fit during model development was a values of greater than 0.98. In some relationships more complex dynamics had to be derived and a second order system with a first order lag and dead time, was used to accurately describe the impulse response (based on the same adequate fit method described above). The equations used for fitting were

$$\frac{y_i(s)}{u_i(s)} = \frac{K_i e^{-\theta_i s}}{\tau_i s + 1} \tag{1}$$

for the first order plus dead time system, and

$$\frac{y_i(s)}{u_i(s)} = \frac{K_i(\tau_{1i} s + 1)e^{-\theta_i s+1}}{(\tau_{2i} s + 1)(\tau_{3i} s + 1)} \tag{2}$$

for the relationships with more complex dynamics.

The fitting curves of two pulse tests are displayed in Figure 3 and Figure 4. An important

thing to note is that the unit of time is minutes, an therefore all responses and analysis will be conducted with this unit for time.

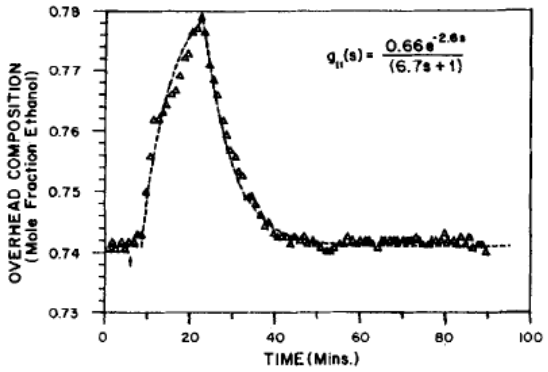

Figure 3: Overhead composition response to a pulse of 15 minutes duration in the reflux rate.

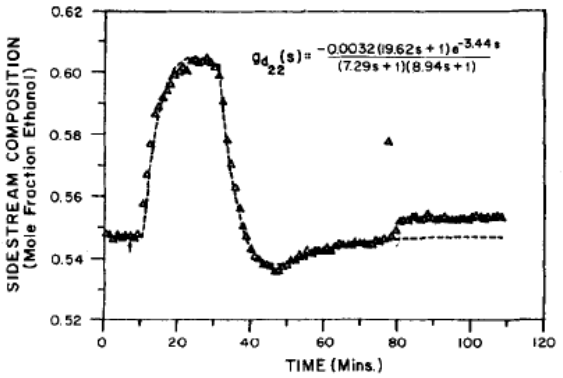

Figure 4: Side stream composition response to a pulse of 15 minutes duration in feed temperature.

The model was then written in the standard form of a linear MIMO system (Ogunnaike et al., 1983),

$$\mathbf{y}(s) = \mathbf{G}(s)\mathbf{u}(s) + \mathbf{G}_d(s)\mathbf{d}(s) \tag{3}$$

where

$$\hat{G}(s) = \begin{bmatrix} G_{11} & G_{12} & G_{13} \\ G_{21} & G_{22} & G_{23} \\ G_{31} & G_{32} & G_{33} \end{bmatrix} = \begin{bmatrix} \frac{0.66e^{-2.6s}}{6.7s+1} & \frac{-0.61e^{-3.5s}}{8.64s+1} & \frac{-0.0049e^{-s}}{9.06s+1} \\ \frac{1.11e^{-6.5s}}{3.25s+1} & \frac{-2.36e^{-3s}}{5.0s+1} & \frac{-0.012e^{-1.2s}}{7.09s+1} \\ \frac{-34.68e^{-9.2s}}{8.15s+1} & \frac{46.2e^{-9.4s}}{10.9s+1} & \frac{0.87(11.61s+1)e^{-s}}{(3.89s+1)(18.8s+1)} \end{bmatrix} \tag{4}$$

and

$$\hat{G}_d(s) = \begin{bmatrix} G_{d11} & G_{d12} \\ G_{d21} & G_{d22} \\ G_{d31} & G_{d32} \end{bmatrix} = \begin{bmatrix} \frac{0.14e^{-12s}}{6.2s+1} & \frac{-0.0011(26.32s+1)e^{-2.66s}}{(7.85s+1)(4.63s+1)} \\ \frac{0.53e^{-10.5s}}{6.9s+1} & \frac{-0.0032(19.62s+1)e^{-3.44s}}{(7.29s+1)(8.94s+1)} \\ \frac{-11.54e^{-0.6s}}{7.01s+1} & \frac{0.32e^{-2.6s}}{7.76s+1} \end{bmatrix} \tag{5}$$

2.6 Scaling the System

In order to perform a controllability analysis on the system, the system had to be scaled according to the method described in Skogestad & Postlethwaite (2001).

In order to perform the scaling operation, the upper and lower limits of all the variables have to be defined. The initial boundary values of all system variables are summarized in Table 2, Table 3, and Table 4.

Table 2: The boundaries of the manipulated variables in the system.

Manipulated Variable	**Lower Constraint**	**Upper Constraint**	**Steady State Value**
u_1, Reflux Flow Rate	0.068	0.245	0.18
u_2, Side Stream Flow Rate	0.00694	0.1	0.046
u_3, Reboiler Steam Pressure	15.6	34	20

Table 3: The boundaries of the controlled variables in the system.

Controlled Variable	**Maximum Set Point Change**	**Steady State Value**
y_1, Overhead Mole Fraction Ethanol	0.05	0.7
y_2, Side Stream Mole Fraction Ethanol	0.1	0.52
y_3, Temperature on Tray #19	8	92

Table 4: The boundaries of the disturbance variables in the system.

Disturbance Variable	**Lower Constraint**	**Upper Constraint**	**Steady State Value**
d1, Feed Flow Rate	0.6	1.1	0.8
d2, Feed Temperature	50	102	78

Using the information above the following matrices can be deduced, that will be used to scale the system

$$D_e = \begin{bmatrix} 0.01 & 0 & 0 \\ 0 & 0.01 & 0 \\ 0 & 0 & 4 \end{bmatrix} \tag{6}$$

$$D_u = \begin{bmatrix} 0.065 & 0 & 0 \\ 0 & 0.03906 & 0 \\ 0 & 0 & 4.4 \end{bmatrix} \tag{7}$$

$$D_d = \begin{bmatrix} 0.3 & 0 \\ 0 & 28 \end{bmatrix} \tag{8}$$

$$r = \begin{bmatrix} 0.05 & 0 & 0 \\ 0 & 0.1 & 0 \\ 0 & 0 & 8 \end{bmatrix} \tag{9}$$

Using the above matrices, the scaled system can be calculated using the following equations from [REF!!!],

$$G = D_e^{-1} \hat{G} D_u \tag{10}$$

$$G_d = D_e^{-1} \hat{G}_d D_d \tag{11}$$

From Equation 10 and Equation 11, the scaled system can be written as

$$G(s) = \begin{bmatrix} G_{11} & G_{12} & G_{13} \\ G_{21} & G_{22} & G_{23} \\ G_{31} & G_{32} & G_{33} \end{bmatrix} = \begin{bmatrix} \frac{4.29e^{-2.6s}}{6.7s+1} & \frac{-2.38266e^{-3.5s}}{8.64s+1} & \frac{-2.156e^{-s}}{9.06s+1} \\ \frac{7.215e^{-6.5s}}{3.25s+1} & \frac{-9.21816e^{-3s}}{5.0s+1} & \frac{-2.156e^{-1.2s}}{7.09s+1} \\ \frac{-0.56355e^{-9.2s}}{8.15s+1} & \frac{0.451143e^{-9.4s}}{10.9s+1} & \frac{1.1(10.1007s+0.87)e^{-s}}{(3.89s+1)(18.8s+1)} \end{bmatrix} \tag{12}$$

and

$$G_d(s) = \begin{bmatrix} G_{d11} & G_{d12} \\ G_{d21} & G_{d22} \\ G_{d31} & G_{d32} \end{bmatrix} = \begin{bmatrix} \frac{4.2e^{-12s}}{6.2s+1} & \frac{-2800(0.028952s+0.0011)e^{-2.66s}}{(7.85s+1)(4.63s+1)} \\ \frac{15.9e^{-10.5s}}{6.9s+1} & \frac{-2800(-0.062784s+0.0032)e^{-3.44s}}{(7.29s+1)(8.94s+1)} \\ \frac{-0.8655e^{-0.6s}}{7.01s+1} & \frac{2.24e^{-2.6s}}{7.76s+1} \end{bmatrix} \tag{13}$$

with

$$R = \begin{bmatrix} 5 & 0 & 0 \\ 0 & 10 & 0 \\ 0 & 0 & 2 \end{bmatrix} \tag{14}$$

3 Controllability Analysis

A full controllability analysis was performed on the system to establish whether:

1. The system has acceptable set point tracking characteristics.
2. The system has acceptable disturbance rejection characteristics.

The method used is described in Skogestad & Postlethwaite (2001).

3.1 Minimal Realisation of the System

The system written in the transfer function notation is in no danger of not being a minimal realizable system. It is only when the system is converted to state space notation it runs the risk of not being a minimal realization.

When converting the transfer function model to a state space realisation of the system, it has to be noted that all dead time that is inherent to the system is ignored, as state space realizations cannot deal with dead time. The system was however converted to its state space realization, in order to cross check the calculated poles and zeros of the system.

The minimum state space realization of the system is given below.

3.2 Functional Controllability

The system has to be checked for functional controllability. This implies that outputs should be able to be controlled independently. There are two factors that have to be considered when checking for functional controllability of a system, namely

1. There have to be at least as many inputs as there are outputs
2. The rank of $G(s)$ should be greater than the number of outputs.

For consideration 1, mentioned above, the number of inputs and outputs in the system is equal. This criteria is therefore satisfied by the system.

For consideration 2, the minimum singular value (or $\underline{\sigma}$) of $G(j\omega)$ should be non-zero. In order to determine whether the system satisfies this criteria, all the singular values, of all the outputs were computed of a wide frequency range. A bode diagram displaying the result can be seem in Figure 5.

As is clear from Figure 5, $\underline{\omega}$ never reaches zero, although it does approach zero as the frequency goes to infinity.

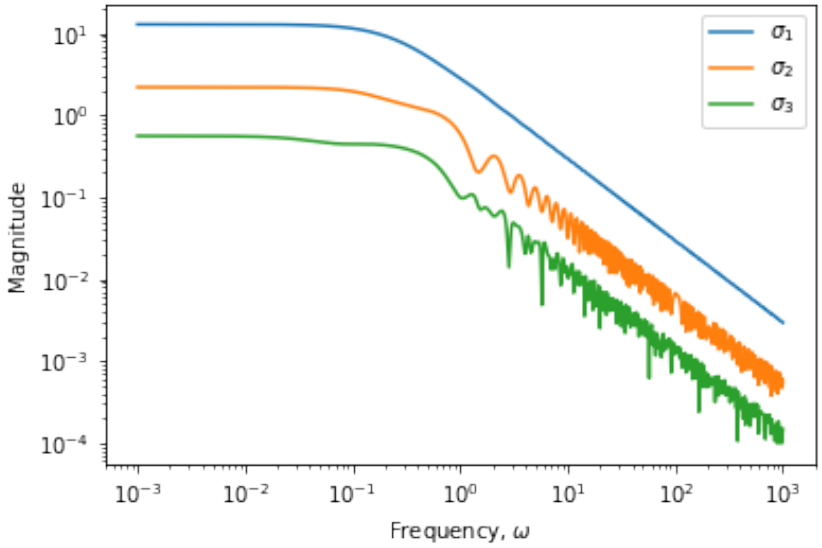

Figure 5: The singular values of $G(j\omega)$.

Based on the above information, it can be concluded that the system is indeed functionally controllable. This implies that the system's rank is equal to the amount of outputs that the system has.

The current selected inputs and outputs can therefore be controlled with adequate independence. This further implies that outputs can return a response by some combination of the input variables.

A system that is functionally uncontrollable will have output responses remaining zero, whenever any combination of an input step function is applied to the system. This therefore results in an output that can in no way be controlled by the inputs, as the inputs do not effect the outputs at all.

3.3 System Poles

3.3.1 Calculating the System Poles

The poles of the system was calculated. The system has a total number of 25 poles. Some of the poles calculated are listed in Table 5. These only contain the more interesting poles. Please refer to Figure 6 for the locations of all the calculated poles.

Table 5: The poles of the system.

Pole	Real Part	Imaginary Part
p_1	-0.31	0
p_2	-0.26	0
p_3	-0.20	0
p_4	-0.23	0
p_5	0.036	0.23
p_6	0.036	-0.23

3.3.2 Calculating the System Pole Directions

The pole directions of the system was calculated by substituting the relevant pole values into $G(s)$ and calculating the input and output directions poles. This was only done for the poles occurring in the Right Hand Plane (RHP). The calculated pole directions are listed in Table 6.

Table 6: The pole directions of the system.

Pole	Input Direction (V)	Output Direction (U)
p_5	$\begin{bmatrix} -0.71 \\ 0.68 + 0.12j \\ 0.13 + 0.05j \end{bmatrix}$	$\begin{bmatrix} -0.19 + 0.22j \\ -0.79 + 0.53j \\ 0.02 - 0.03j \end{bmatrix}$
p_6	$\begin{bmatrix} -0.71 \\ 0.68 - 0.12j \\ 0.13 - 0.05j \end{bmatrix}$	$\begin{bmatrix} -0.19 - 0.22j \\ -0.79 + 0.53j \\ 0.02 - 0.03j \end{bmatrix}$

Table 7: The pole directions of the system in phasor notation.

Pole	Input Direction (V)	Output Direction (U)
p_5	$\begin{bmatrix} 0.71\angle 0^\circ \\ 0.69\angle 10.1^\circ \\ 0.13\angle 19.6^\circ \end{bmatrix}$	$\begin{bmatrix} 0.29\angle 130.9^\circ \\ 0.96\angle 146.0^\circ \\ 0.04\angle -48.9^\circ \end{bmatrix}$
p_6	$\begin{bmatrix} 0.71\angle 0^\circ \\ 0.69\angle -10.1^\circ \\ 0.13\angle -19.6^\circ \end{bmatrix}$	$\begin{bmatrix} 0.29\angle -130.9^\circ \\ 0.96\angle -146.0^\circ \\ 0.04\angle 48.9^\circ \end{bmatrix}$

3.3.3 Discussion of System Poles

All the calculated system poles are in the open left hand plane (LHP). From this it can be concluded that the open loop system is stable. The complex poles that lie close to zero on the real axis, may pose to be of some concern. Further stability analysis of the system will shed some light regarding this. The locations of the poles of the system can be seem in Figure 6.

Although the directions of the poles are calculated and displayed in Table 6, the directions are not entirely relevant, as they will not cause the system to become unstable. The open loop system of $G(s)$ is therefore stable for any input direction.

3.4 System Zeros

3.4.1 Calculating the System Zeros

The system zeros were calculated. The system contains a total number of nine zeros, all of them located in the left hand plane (LHP). The system zeros are given in Table 8.

Table 8: The zeros of the system.

Zero	Real Part	Imaginary Part
z_1	-0.3077	0
z_2	-0.2571	0
z_3	-0.2	0
z_4	-0.1493	0
z_5	-0.1227	0
z_6	-0.1157	0
z_7	-0.1104	0
z_8	-0.0917	0
z_9	-0.0532	0

3.4.2 Calculating the System Zero Directions

The zero directions of the system was calculated by substituting all the zero values into $G(s)$ and calculating the input and output directions of the relevant zeros using the singular value decomposition of $G(z_i)$. The calculated zero directions are given Table 9.

Table 9: The zero directions of the system.

Zero	Input Direction (V)	Output Direction (U)
z_1	$\begin{bmatrix}1\\0\\0\end{bmatrix}$	$\begin{bmatrix}0\\1\\0\end{bmatrix}$
z_2	$\begin{bmatrix}0\\0\\1\end{bmatrix}$	$\begin{bmatrix}0\\0\\1\end{bmatrix}$
z_3	$\begin{bmatrix}0\\-1\\0\end{bmatrix}$	$\begin{bmatrix}0\\1\\0\end{bmatrix}$
z_4	$\begin{bmatrix}-1\\0\\0\end{bmatrix}$	$\begin{bmatrix}-1\\0\\0\end{bmatrix}$
z_5	$\begin{bmatrix}-1\\0\\0\end{bmatrix}$	$\begin{bmatrix}0\\0\\1\end{bmatrix}$
z_6	$\begin{bmatrix}0\\1\\0\end{bmatrix}$	$\begin{bmatrix}-1\\0\\0\end{bmatrix}$
z_7	$\begin{bmatrix}0\\0\\1\end{bmatrix}$	$\begin{bmatrix}-0.707\\-0.707\\0\end{bmatrix}$
z_8	$\begin{bmatrix}0\\1\\0\end{bmatrix}$	$\begin{bmatrix}0\\0\\1\end{bmatrix}$
z_9	$\begin{bmatrix}0\\0\\1\end{bmatrix}$	$\begin{bmatrix}0\\0\\1\end{bmatrix}$

3.4.3 Discussion of System Zeros

The system zeros exists for values of s where the system $G(s)$ loses rank. The zeros calculated, are transmission zeros of the system as they do not relate to the zeros of the elements that make up the transfer function matrix $G(s)$. It is clear that there are no RHP zeros, and no further analysis of the zeros are required, as there are no limitations imposed by Left Hand Plane (LHP) zeros.

LHP zeros will mostly cause high overshoots during control, but this does not pose as a stability concern for the system and will in no way limit the bandwidth of the system.

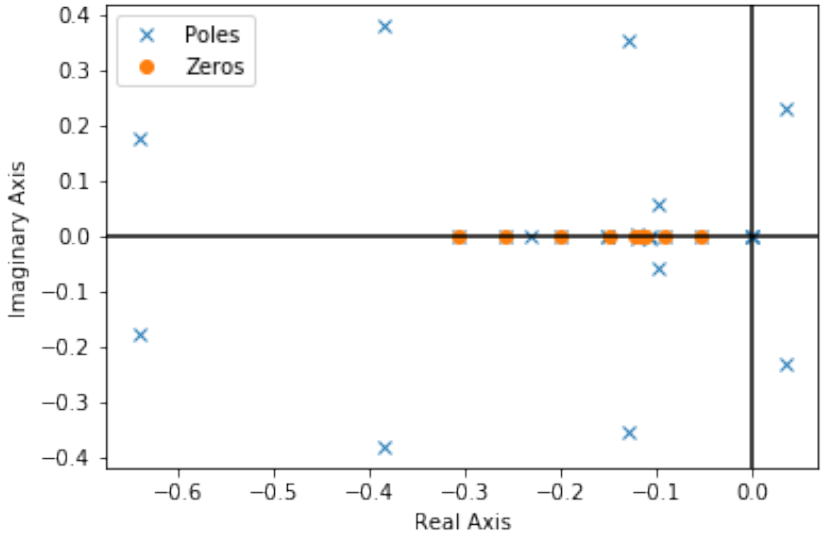

Figure 6: A graphical representation of the system's poles and zeros.

3.5 RGA Values of the System

The Routh Gain Array (RGA) of $G(j\omega)$ was calculated, for all values of ω. This enables the analysis of RGA values not only for at the crossover frequencies, but at all other frequencies to thoroughly check for large RGA elements that will render a plant that is difficult to control. The calculated RGA analysis can be seen in Figure 7.

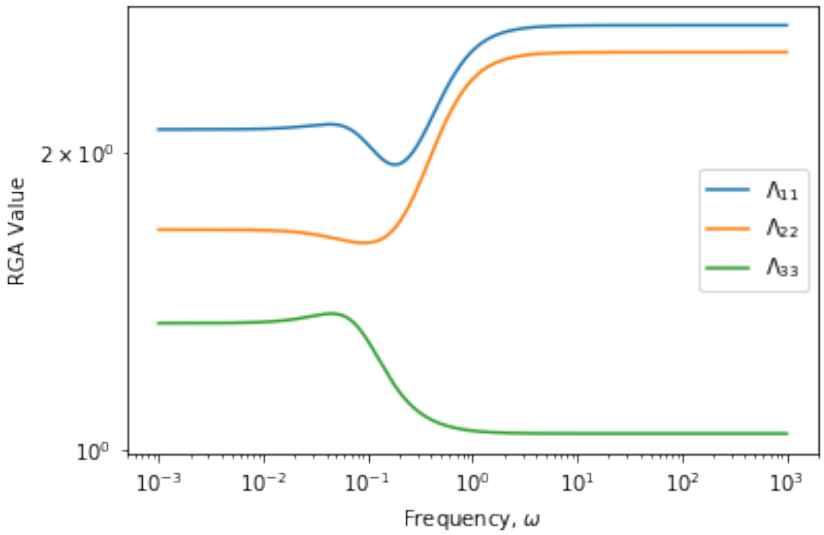

Figure 7: The diagonal values of RGA matrix, Λ, over a wide range of frequencies.

To verify that the off-diagonal values remain within acceptable ranges, the RGA of $G(0)$ and $G(j\omega)$ with $\omega = 10^3$ was calculated. The two matrices calculated are

$$\Lambda G(0) = \begin{bmatrix} 2.11 & -0.84 & -0.26 \\ -0.59 & 1.67 & -0.08 \\ -0.52 & 0.17 & 1.34 \end{bmatrix} \tag{15}$$

$$\Lambda G(j10^3) = \begin{bmatrix} 2.69 & -1.63 & -0.03 \\ -1.52 & 2.53 & -0.01 \\ -0.17 & 0.13 & 1.04 \end{bmatrix} \tag{16}$$

3.6 Singular Values of the System

The minimum singular value is a useful tool when doing controllability an analysis. The minimum singular value for this system is depicted in Figure 5.

The minimum singular value should be as large as possible, especially at frequencies where control is needed (Skogestad & Postlethwaite, 2001).

From Figure‘5, it is clear that

$$\underline{\sigma}(G(j\omega)) < 1, \forall\omega \tag{17}$$

This implies that it is not possible to make output changes of unit magnitude, by using inputs of unit magnitude for any values of ω.

This is bad from a controllability point of view, especially when considering set-point tracking. When tracking set-points, outputs ideally have to controlled by making single set-point changes. This enables the use of a decentralized controller. An example of such a controller (represented in a standard transfer function notation) is

$$K(s) = \begin{bmatrix} \frac{K_1}{\tau_1 s+1} & 0 & 0 \\ 0 & \frac{K_2}{\tau_2 s+1} & 0 \\ 0 & 0 & \frac{K_3}{\tau_3 s+1} \end{bmatrix} \tag{18}$$

With the current plant configuration and design, the use of a decentralized controller is possible, but adequate set-point tracking will not be possible as the outputs will not reach the set-points on the high and/or low set-point values.

For example; when the temperature on tray # 19 , y_3, is controlled between 88 and 96 °, set-point tracking by manipulation of the stream feed pressure, u_3, will be acceptable (when considering a decentralized controller that contains an integral component). Acceptable set-point tracking includes: fast response time, elimination of error, robust responses. An adequately fast response time for this system will be around 45 minutes. With a high enough gain value, K_{c3}, this will be achieved. The integral component of the controller will eliminate the error completely over time, given that the integral component of the controller, τ_{c3}, is large enough. Robust control will be achieved by tuning the controller values after initial implementation.

Now, when considering set-points on the outer limits of the control range for y_3, the control system will not perform acceptably. For instance when the set-point of y_3 is set to ranges 84 to 88 °C or 96 to 100 °C, the response time of the set-point change may still be good, but the error will not be able to be cancelled. This is due to the minimum singular value of the system being smaller than 1. The unit change in the input, u_3, will not cause a unit change in the output, y_3. Since the system is scaled, this simply means that the outer set-points cannot be reached by only manipulating one input variable.

The situation discussed above, only applies to the y_3 and u_3 control pairing. From Figure 5, it is clear that the criteria stated in Equation 17 is satisfied for the y_2 and u_2 paring for all frequencies where $\omega < 0.28$. Similarly, the criteria in Equation 17 is satisfied in the y_1 and u_1 pairing for all frequencies where $\omega < 2.97$.

The are a few options for improvement and successful implementation of the control system. They are

1. To implement a controller that is not decentralised. This controller can still control y_1 an y_2 using u_1 and u_2. y_3 will then be controlled by a combination of u_3 and u_2 (this follows from the RGA matrix analysis, where u_1 is negative with regard to y_3). The controller equation will then take the form of

$$K(s) = \begin{bmatrix} \frac{K_1}{\tau_1 s+1} & 0 & 0 \\ 0 & \frac{K_2}{\tau_2 s+1} & 0 \\ 0 & \frac{K_{3_1}}{\tau_{3_1} s+1} & \frac{K_{3_2}}{\tau_{3_2} s+1} \end{bmatrix} \tag{19}$$

   While this will ensure that acceptable set-point tracking of the bottom tray temperature is accomplished, there will be a loss in the performance and robustness of the control in the side-stream composition.

2. Increase the size of the control valves controlling the stream pressure. This will

increase the overall gain in the system, shifting the singular values in an upward direction. This will render acceptable set-point tracking of all parameters.

3. Lower the required range wherein set-point tracking has to be performed.

3.7 System Bandwidth

The bandwidth of the system is the maximum frequency where sensible control can still be implemented. Mathematically it is where the sensitivity function of the system first crosses $1/\sqrt{2}$, or

$$|S(j\omega)| = \frac{1}{\sqrt{2}} \tag{20}$$

Since no controller is implemented as yet, there is no way of calculating the sensitivity function. As discussed in Section 3.3 and Section 3.4, there are no Right Hand Plane (RHP) poles or zeros in this system. There are therefore no special bandwidth limitations on the system due to these parameters.

The system does however contain a lot of dead time. There is dead time in each transfer function, as this is it is inherent to the fitting function used to build the model. There are constraints on the bandwidth due to this dead time. To visualize the dead time inherent to the system, please refer to Equation 21. This equation, simply named the dead time matrix, is a representation of the dead time elements (θ) for the respective transfer functions.

$$\Theta = \begin{bmatrix} 2.6 & 6.5 & 9.2 \\ 3.5 & 3.0 & 9.4 \\ 1.0 & 1.2 & 1.0 \end{bmatrix} \tag{21}$$

The lower bound time delay for each output (or contained within each row of Θ) is of interest. This is because the minimum time for any input to effect the relevant output (θ_i^{min}), can be seen as the delay that is pinned to output y_i. Alternatively this statement can be represented mathematically as

$$\theta_i^{min} = \min_j \theta_{ij} \tag{22}$$

The bandwidth of input u_i is then limited by $1/\theta_i$. Table 10, contains a summary of the bandwidth limitations of the system.

Input	Theta	Bandwidth
y_1	2.6	0.38
y_2	3.0	0.33
y_3	1.0	1.0

Table 10: Bandwidth limitations imposed by time delays.

While these limitations are in no way ideal, the do not pose to be a major threat for the control of the system. There are a few conclusions that can be drawn from this, namely

1. When looking at Equation 21 together with Section 3.5, it is clear that the diagonal elements that are paired in the RGA matrix, also contain the least amount of dead time. This is good, as it is obvious that you want to control a variable with an input that does not take long to effect the variable. Pairing of the variables are therefore made relatively straight forward.

2. The delays imposed are not that significant when considering the desired response times for the control system. Required response times for the variables of the distillation column range between 30 and 60 minutes. The maximum delay calculated here (3 minutes), is relatively small and a low gain controller should be able to control the system with adequate performance. The performance of the system is discussed in more detail later in the report.

3.8 Disturbance Rejection

In order for the system to successfully reject disturbances, tight control and large bandwidths are required to when disturbances are large or "fast".

To evaluate a MIMO system's ability to reject disturbances, the disturbance directions have to be evaluated (which is not the case when considering a SISO system).

The model contains two disturbances, each having it's own associated direction. The disturbance directions are defined as

$$y_d = \frac{1}{||g_d||_2} g_d \tag{23}$$

where g_d represents the effect of a single disturbance on the outputs ($y = g_d d$).

The disturbance directions for both disturbances were evaluated for all frequencies. The results can be seem in Figure 8.

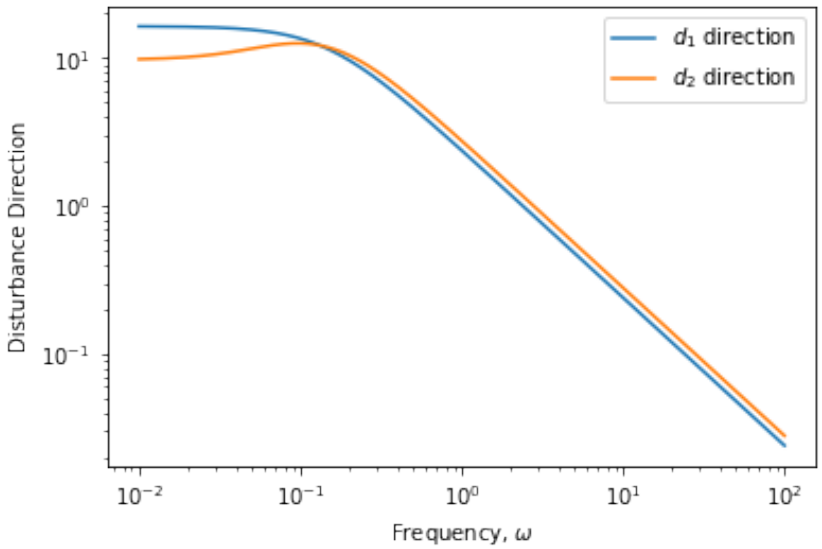

Figure 8: The disturbance directions as a function of frequency.

Now, following that the system has been scaled (Section 2.6), we can say that the worst-case disturbance to be selected is $|d_i(\omega)| = 1$. Using this, and the fact that with feedback control we have $e = Sg_d d$, the disturbance performance objectives are then satisfied when

$$||Sg_d||_\infty < 1 \tag{24}$$

Note that $S(s)$ could not actually be calculated. This is because no controller has yet been designed for the system. To gain better understanding of the disturbances in the system, a proportional decentralized controller with a gain of 1 (for all elemnts) was used.

Skogestad & Postlethwaite (2001) used the above and derived tight bounds on the sensitivity function and loop gain for MIMO syste, considering the disturbance directions as well. For the system to adequately reject disturbances, we at least require that

$$\underline{\sigma}(S) < \frac{1}{||g_d||_2} \tag{25}$$

Where S is the sensitivity function of the transfer function model, or can be given mathematically as

$$S = (I + G)^{-1} \tag{26}$$

for a negative feedback loop.

Equation 25 can be represented graphically. The left-hand side and right-hand side of the equation was plotted for all values of ω. The results are displayed in Figure 9.

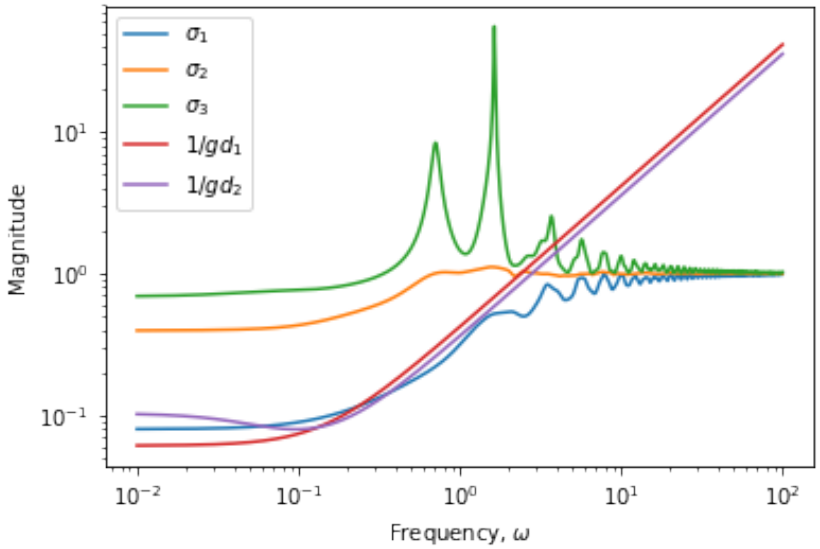

Figure 9: The disturbance directions with respect to the singular values of the sensitivity of $G(s)$, $S(s)$.

From Figure 9, it is clear that, based on the criteria stated in Equation 25, there may be some problems regarding disturbance rejection (especially at low frequencies). To share more light on the causes of the problem, an more in depth analysis is conducted below.

3.9 Disturbances and Input Saturation

3.9.1 Analysis for Perfect Control

Here it is asked whether disturbance rejection is possible, without input saturation ($||u|| < 1$). There are two methods of evaluating this, by use of

1. The max-norm.
2. The two norm.

As the system is square, the max-norm can be used to analyse this plant. Disturbances are analysed separately, and combined to gain full understanding of how the disturbances will effect the controller input.

When considering single disturbances, input saturation is avoided (and perfect control is achieved) when

$$||G^{-1}g_d||_{max} < 1 \tag{27}$$

and when considering simultaneous disturbances the requirement can be rewritten to

$$||G^{-1}G_d||_{i\infty} < 1 \tag{28}$$

where $||\cdot||_{i\infty}$ is the induced max-norm defined as

$$||A||_{i\infty} = \max_j \left(\sum_i |a_{ij}| \right) \tag{29}$$

The criteria stated above is displayed in Figure 10.

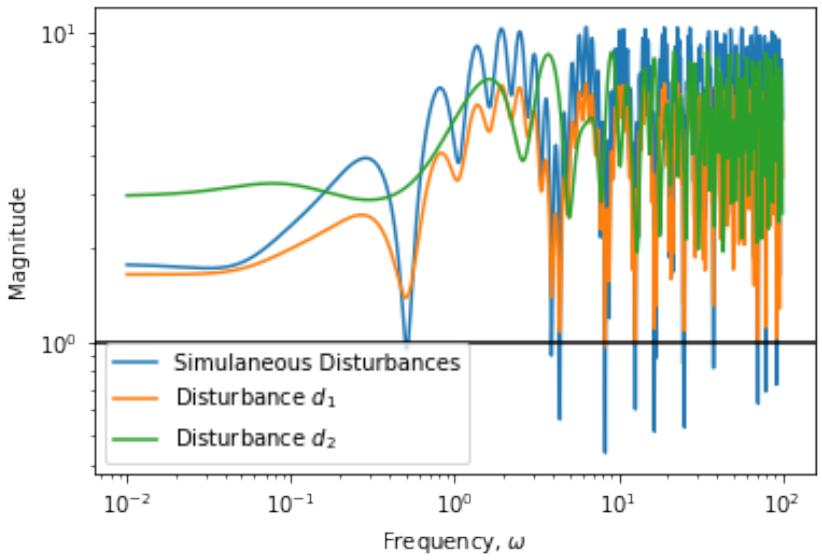

Figure 10: The effect of disturbances on input saturation.

From Figure 10, it is clear that perfect control is not possible for either disturbance, or even for a combination of both. The disturbance d_2 is the most problematic, as the

disturbance causes $||G^{-1}g_d||_\infty||$ to be greater than 1 for all values of frequency. Perfect control of this disturbance is not possible.

Input saturation is therefore unavoidable. This does not necessarily mean that the plant is uncontrollable with regard to disturbance rejection. An analysis for acceptable disturbance rejection with regard to input saturation has to be performed.

3.9.2 Analysis for Acceptable Control

Acceptable control exists when, for the response $e = Gu + G_d d$ it is possible achieve $||r|| \leq 1$ for any $||d|| \leq 1$ using inputs $||u|| \leq 1$. Only the max-norm is used in this section. The conditions resulting from the analysis are for achieving $||e|| \leq 1$ (the minimum requirement).

The criteria derived by Skogestad & Postlethwaite (2001) for system to exhibit acceptable control characteristics is given as

$$\sigma_i(G) \geq |u_i^H g_d| - 1, \text{ at frequencies where } |u_i^H g_d| > 1 \tag{30}$$

Figure 11, Figure 12 and Figure 13 are the graphical representations of the criteria stated in Equation 30 for the three different input directions. The effect of both disturbances are plotted against the singular value for the specific input. This will help to gain insight into the way that disturbances effect the input values to the controller.

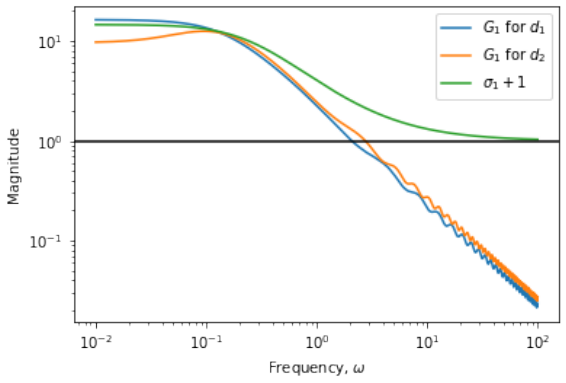

Figure 11: Graphical representation of criteria outlined in Equation 30, for e_1

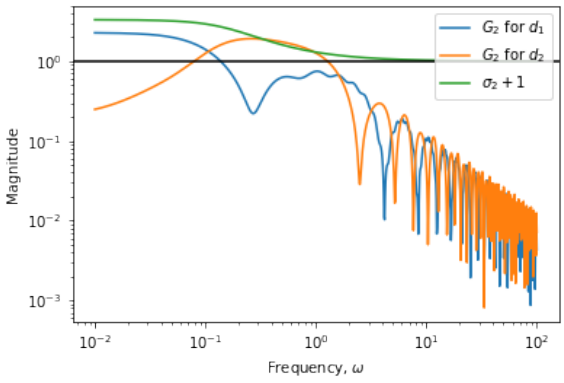

Figure 12: Graphical representation of criteria outlined in Equation 30, for e_2

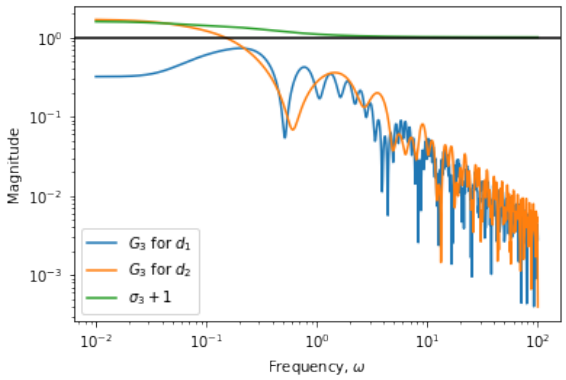

Figure 13: Graphical representation of criteria outlined in Equation 30, for e_3

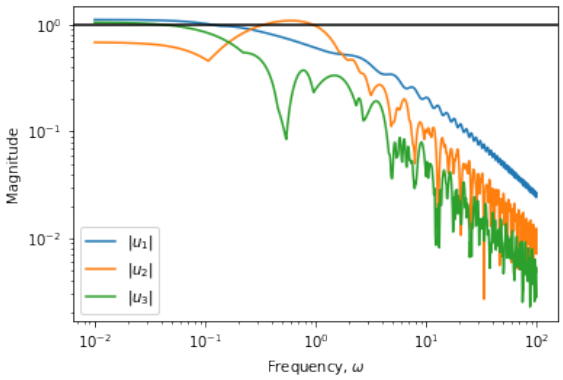

Figure 14: The required controller input values for the worst case

When considering Figure 11, it is clear that the input into the controller (controlling y_1) is saturated at low frequencies. This is due to the effects that d_1 has on the system. It is clear that a maximum change in the feed flow rate, will result in the reflux flow rate flow being saturated. This translates to a fully open or fully closed control valve in this section of the plant. There are two solutions to the problem, namely

1. Install a bigger control valve (and therefore line size) on the reflux stream. This change will impact the mathematical model by changing the gain and response times in the first row of transfer function matrix $G(s)$. This speed up the dynamics of the system, and result in higher minimum singular values for $S(s)$, especially at low frequencies where the problem is experienced. Better disturbance rejection will result.

2. Lower the maximum designed for disturbance size. This can be done by tighter control upstream from the distillation column (by the flow regulator/controller indicated in Figure 2).

Both actions will take considerable time to implement, as the effect of tighter flow control will effect the reactor vessel's control as well. A bigger, or more sophisticated control valve, will have a installation cost, as well as a downtime, as well as recommissioning of the system, production cost implication.

From Figure 12 it is clear that acceptable control is possible, since the second input to the controller is saturated by neither disturbance changes (for all frequencies).

Regarding Figure 13, it is clear that disturbance rejection is again not acceptable, as the third input to the controller (e_3) is saturated when disturbance d_2 is at it's maximum feed

value. When relating back to the physical process, this means that the stream pressure control valve, fully closes when the feed temperature rises to 106 °F or fully opens when the feed temperature drops to 58 °F. To solve this problem there again exists a few solutions, namely

1. Increase the size of the control valve. When doing this, it is imperative that the compressors in the stream line's design also be reviewed, as it may be required that a higher stream flow rate be required at the lowest disturbance value. The major downside of this option, is that there is no compensation for when the feed temperature rises to the maximum disturbance value. Even the bigger control valve will still fully close.

2. Decrease the disturbance limit values. This is again the most straightforward method to increase the effectiveness of disturbance rejection over the distillation column. This can be done by implementing tighter control over the feed heat exchanger unit (indicated in Figure 2). Methods to implement tighter control will be to increase the controller gain of the unit (an decreasing the amount of integral control). Implementing a feed forward controller on the heat exchanger unit by adding the working fluid's temperature as measured variable is another option (although this will not be the most cost effective solution).

3. Change the controlled variable y_3. By changing the controlled variable y_3 from the temperature on tray #19, to the boil-up ratio will reduce the response time in dynamics of the third row in $G(s)$. This will lead to higher singular values in $S(s)$, especially at low frequencies, and disturbance rejection performance criteria will be met. This solution has the downside that the bottoms composition will not be controlled directly. Since the production is more interested in the quality of the distillate composition (as this is where the ethanol product is), this is not a major loss and the solution can be considered. A full controllability analysis will have to be conducted on the new system if this is the chosen solution, as the dynamics of the whole MIMO transfer function model will change.

Figure 14 illustrates the required input variables (u_i) for maximum disturbance rejection. The figure reiterates the problems experienced in Figure 11 and Figure 13, where the inputs required for disturbance rejection will saturate the controller.

4 Changing the System Bounds

4.1 Disturbance Rejection and Input Saturation

This section will look at the proposed changes stated in Section 3.9.2. Since there is no information on the current controllers and final control elements employed on site, investigation into changes of the control hardware will not be conducted. This is purely due to

1. Lack of information about current control infrastructure.
2. Lack of a first principles mathematical model, or Aspen simulation where the sizes of the control elements can be changed at will without any additional cost.

The proposed changes to the perimeters of the control system will therefore be investigated. As mentioned in Section 3.9.2, disturbance rejection is required for a too high range of both disturbances. In order to rectify the situation, the ranges where adjusted. This in turn caused the scaled system to change, and new responses resulted. Table 11 contains more information with regard to the proposed ranges.

Table 11: The new proposed boundaries of the disturbance variables in the system.

Disturbance Variable	Lower Constraint	Upper Constraint	Steady State Value
d1, Feed Flow Rate	0.65	1.0	0.8
d2, Feed Temperature	60	95	78

This led to a new scaling matrix

$$D_d = \begin{bmatrix} 0.2 & 0 \\ 0 & 18 \end{bmatrix} \tag{31}$$

and a new disturbance matrix

$$G_d(s) = \begin{bmatrix} G_{d11} & G_{d12} \\ G_{d21} & G_{d22} \\ G_{d31} & G_{d32} \end{bmatrix} = \begin{bmatrix} \frac{2.8e^{-12s}}{6.2s+1} & \frac{-1800(0.028952s+0.0011)e^{-2.66s}}{(7.85s+1)(4.63s+1)} \\ \frac{10.6e^{-10.5s}}{6.9s+1} & \frac{-1800(-0.062784s+0.0032)e^{-3.44s}}{(7.29s+1)(8.94s+1)} \\ \frac{-0.577e^{-0.6s}}{7.01s+1} & \frac{1.44e^{-2.6s}}{7.76s+1} \end{bmatrix} \tag{32}$$

The same mathematical procedure is then followed as outlined in Section 3.9.2, to establish whether acceptable disturbance rejection can take place. The following figures result.

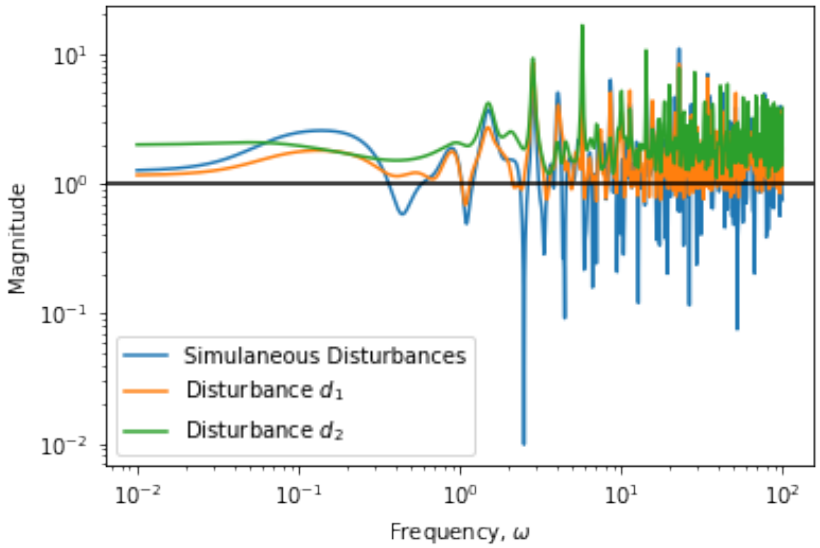

Figure 15: The effect of disturbances on input saturation.

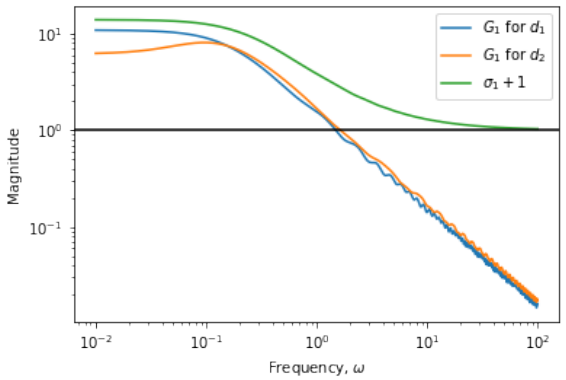

Figure 16: Graphical representation of criteria outlined in Equation 30, for e_1

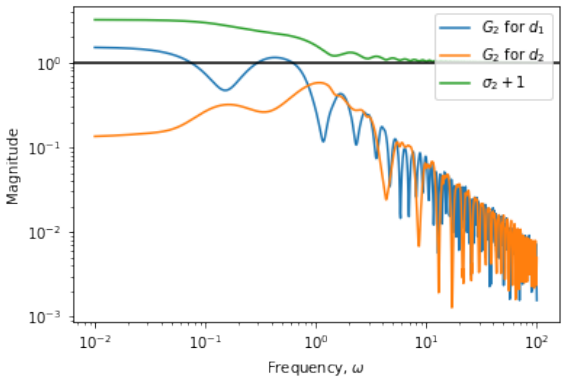

Figure 17: Graphical representation of criteria outlined in Equation 30, for e_2

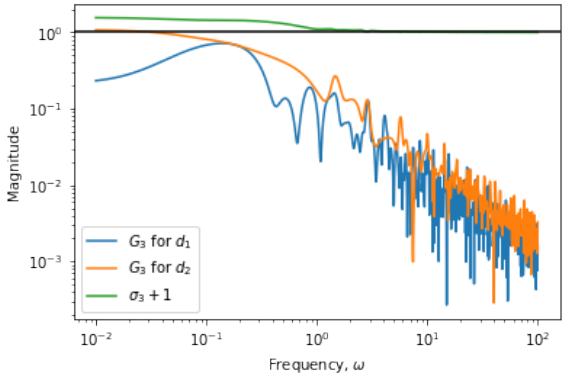

Figure 18: Graphical representation of criteria outlined in Equation 30, for e_3

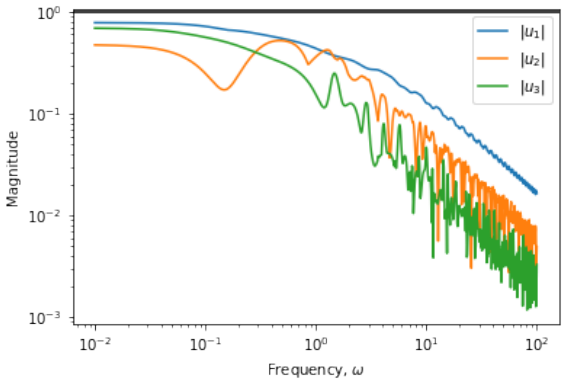

Figure 19: The required controller input values for the worst case

References

Ogunnaike, BA, Lemaire, JL, Morari, M and Ray, WH (1983) "Advanced Multivariable Control of a Pilot Plant Distillation Column" *AIChE Journal*, *29 (4)*, 632 *639*.

Skogestad, S and Postlethwaite, I (2001) *Multivariable Feedback Control: Analysis and Design*, 2nd ed. John Wiley & Sons, New York.